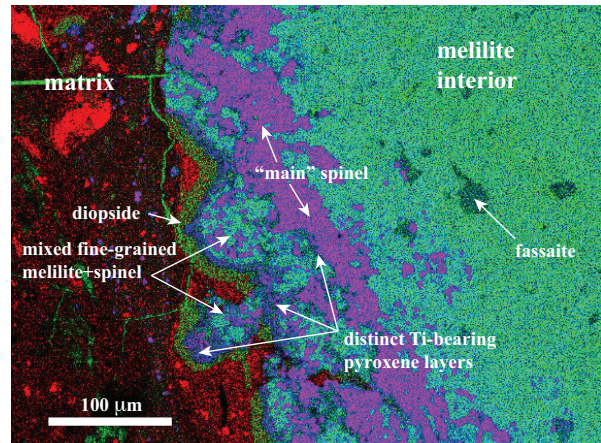


**HETEROGENEOUS OXYGEN ISOTOPIC COMPOSITION OF A COMPLEX WARK-LOVERING RIM AND THE MARGIN OF A REFRACTORY INCLUSION FROM LEOVILLE.** J. I. Simon<sup>1</sup>, J. E. P. Matzel<sup>2</sup>, S. B. Simon<sup>3</sup>, P. K. Weber<sup>2</sup>, L. Grossman<sup>3</sup>, D. K. Ross<sup>1,4</sup>, and I. D. Hutcheon<sup>2</sup>. <sup>1</sup>Center for Isotope Cosmochemistry and Geochronology, ARES NASA-JSC, Houston, TX 77058, USA (Justin.I.Simon@NASA.gov), <sup>2</sup>LLNL, Livermore, CA 94551, USA, <sup>3</sup>The University of Chicago, Chicago, IL 60637, USA, <sup>4</sup>Jacobs Tech., TX 77058, USA.

**Introduction:** Wark-Lovering (WL) rims [1] surrounding many refractory inclusions represent marker events in the early evolution of the Solar System in which many inclusions were exposed to changes in pressure [2], temperature [3], and isotopic reservoirs [4-7]. The effects of these events can be complex, not only producing mineralogical variability of WL rims [2], but also leading to mineralogical [8-10] and isotopic [7, 11, 12] changes within inclusion interiors. Extreme oxygen isotopic heterogeneity measured in CAIs has been explained by mixing between distinct oxygen gas reservoirs in the nebula [13]. Some WL rims contain relatively simple mineral layering and/or are isotopically homogeneous [14, 15]. As part of a larger effort to document and understand the modifications observed in some CAIs, an inclusion (L6) with a complex WL rim from Leoville, a member of the reduced CV3 subgroup was studied. Initial study of the textures and mineral chemistry was presented by [16]. Here we present NanoSIMS oxygen isotopic measurements to complement these petrologic observations.

**Sample:** L6 is a pristine compact Type A (CTA) inclusion with clusters of spinel (typically euhedral, ~50  $\mu\text{m}$  across) and fassaite grains (anhedral) enclosed in visually unaltered melilite that exhibits normal compositional zoning ( $\text{Åk}_{3-30}$ ) within the margin (~200  $\mu\text{m}$ ) of the inclusion [16]. At the edge of the inclusion is a nearly continuous and often thick (up to 100  $\mu\text{m}$ ) layer of spinel intergrown with the melilite interior. Outside of the main spinel layer are additional layers composed of pyroxene  $\pm$  melilite. Based on petrography and mineral chemistry [16], five generations of pyroxene were identified in the WL rim. In the section studied herein, the innermost is Ti-bearing (Ti-pyx) and appears intergrown with the “main” spinel layer. This Ti-pyx ( $\leq 10 \mu\text{m}$ ) becomes less Ti-rich outward and is intergrown with a mixed layer of fine-grained melilite and spinel of varying thickness. Locally the fine-grained melilite layer has a range of grain sizes and can be found in contact with the “main” spinel layer. Coarser melilite tends to enclose less spinel. In places, a second Ti-pyx-melilite layer exists with a distinct Ti-pyx composition from the first [16]. Finally, the entire inclusion and complex rim is surrounded by a uniform layer of diopside (~15  $\mu\text{m}$ ), in some places in direct contact with Ti-pyx from an inner layer and sometimes directly

overlying the irregular fine-grained mixed melilite-spinel layer (Fig. 1).



**Figure 1.** Mg (red), Ca (green), Al (blue) X-ray image of L6 exhibiting a “simple” example of the Wark-Lovering rim stratigraphy surrounding the inclusion.

**Methods:** We used the LLNL NanoSIMS 50 to perform oxygen isotopic measurements following published methods [7]. Data come from multiple traverses across the rims and outer margin of the interior of L6 to define oxygen isotopic zoning profiles. Data points are ~2  $\mu\text{m}$  diameter single-phase analyses as evaluated by their  $^{28}\text{Si}/^{16}\text{O}$  ion ratios and SEM imagery after the NanoSIMS measurements. Oxygen isotope compositions are reported as  $\Delta^{17}\text{O} = \delta^{17}\text{O} - 0.52\delta^{18}\text{O}$ , which represents the departure from the terrestrial mass fractionation (TMF) line that defines the terrestrial oxygen reservoir. Based on standard analyses, the precision is <3%/amu ( $2\sigma$ ). We evaluated instrumental mass fractionation (IMF) and reproducibility by repeat analyses of spinel, anorthite, grossular, pyroxene, and forsterite standards. The difference in  $\Delta^{17}\text{O}$  among the terrestrial standard minerals was similar to our typical uncertainty (~3.0%). Mineral compositions, and X-ray and backscattered electron maps were used to guide NanoSIMS traverses and verify the mineralogy of analysis spots.

**Results:** Oxygen isotope data come from traverses spanning the WL rims and/or margin of the interior (Fig. 2). Like several CAIs studied previously [7, 17, 18], L6 exhibits large variations in  $\Delta^{17}\text{O}$  (>20‰). Compared to the inclusion reported by [7], interior melilite in L6 is more homogeneous and  $^{16}\text{O}$ -poor ( $\Delta^{17}\text{O} \sim -6\text{‰}$ ). The exception is a systematic  $\Delta^{17}\text{O}$  de-

crease from  $\sim -6\%$  to  $-22\%$  at the edge. Spinel in the “main” layer at the margin are  $^{16}\text{O}$ -rich ( $\Delta^{17}\text{O} \leq -25\%$ ). The Ti-pyx layers have intermediate  $\Delta^{17}\text{O}$  compositions ( $\Delta^{17}\text{O} \sim -14$  to  $-18\%$ ). Melilite from the mixed layer exhibits extreme oxygen isotopic heterogeneity with  $\Delta^{17}\text{O}$  values ranging from  $\sim -6\%$ , like a majority of the interior crystals, to  $-27\%$  in one melilite. Diopside in the outermost layer exhibits less variability with  $\Delta^{17}\text{O}$  from  $-15\%$  to  $-23\%$ .

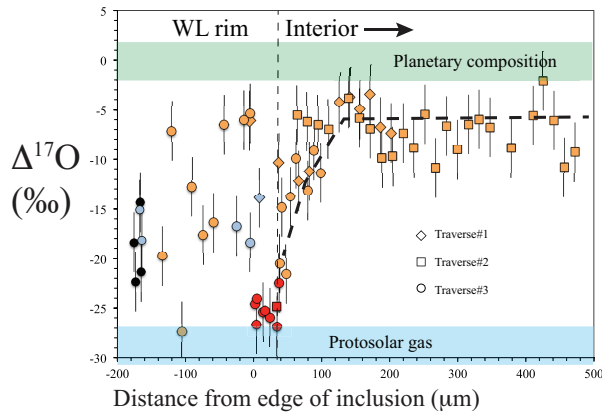


**Figure 2.** Oxygen isotopic zoning across the Wark-Lovering rim layers and melilite margin of L6 obtained by NanoSIMS. Individual traverses are identified by symbol; melilite analyses are tan, spinel red, Ti-pyx blue, and diopside black. Thick dashed curve emphasizes the oxygen isotopic zoning in melilite at the margin of L6. Spinel and the most  $^{16}\text{O}$ -rich rim melilite match the oxygen isotope composition of [19] and likely represent the protosolar composition.

**Discussion:** The fine-scale spatial zoning and textural features create concern if the mineral analyses represent pure phases. A quantitative means to evaluate this possibility is shown in Fig. 3 where we plot the  $^{28}\text{Si}/^{16}\text{O}^-$  secondary ion ratio versus distance for the data shown in Fig. 2; data are not corrected for differences in ion yield. If the  $^{16}\text{O}$ -rich composition of melilite was due to overlap of the primary beam onto spinel, the  $^{28}\text{Si}/^{16}\text{O}^-$  ratio would show marked changes from the  $\sim 0.02$  value consistent with pure melilite.

Oxygen isotope compositions within the interior and compositional zoning at the margin of L6 show great similarity to a previously studied CAI (Ef-1), a CTA from Efremovka [17]. The WL rim on L6 is much more complicated (both mineralogically and isotopically). The oxygen isotopic compositions of the WL rim phases share some similarity to previously studied WL rims [7, 17], e.g., spinel is generally  $^{16}\text{O}$ -rich while pyroxene has intermediate  $\Delta^{17}\text{O}$  values. The wealth of melilite data from a WL rim is new, as is the extreme O-isotope heterogeneity. Three Ti-pyx layers seen in [16] appear to have similar oxygen isotopic compositions to one another, indicating that there were

more cycles of deposition than recorded by isotopic differences. The average diopside  $\Delta^{17}\text{O}$  value is slightly more  $^{16}\text{O}$ -rich than the average Ti-pyx value (from any or all inner Ti-pyx layers). Likewise, melilite in the WL-rim exhibits a general inward trend towards  $^{16}\text{O}$ -poor values despite the existence of  $^{16}\text{O}$ -rich melilite at the edge of the inclusion. Although it is assumed that the inclusion formed from an  $^{16}\text{O}$ -rich protosolar gas [19], the general sense of zoning in the WL-rim, as well as the zoning in melilite at the margin of the inclusion, suggest that the inclusion progressively exchanged or formed from  $^{16}\text{O}$ -poor and then  $^{16}\text{O}$ -rich reservoirs. The heterogeneity within the interior supports our previous conclusion that CAIs record a progressive trend in the extent of exchange with a number of isotopically distinct reservoirs that is decoupled from mineralogical evidence of secondary alteration [17]. The WL rim and interior data support models in which CAIs were transported between at least two distinct nebular gases multiple times, e.g., [7].

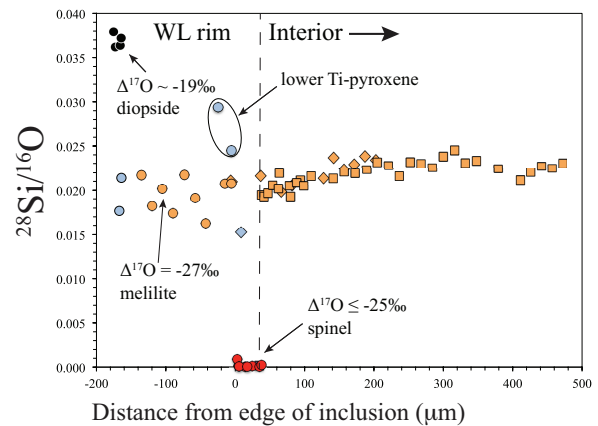


**Figure 3.**  $^{28}\text{Si}/^{16}\text{O}$  ion ratio profile across the minerals in the Wark-Lovering rim layers and interior of L6 used to identify data that could come from analytical mixtures. Spurious data are not shown (see text). Shifts in  $^{28}\text{Si}/^{16}\text{O}$  among melilite and between innermost high Ti-pyx, lower Ti-pyx, and diopside, combined with  $\Delta^{17}\text{O}$  indicate negligible contamination from spinel and are those generally expected from their chemical compositions. Symbols are as in Fig. 2.

**References:** [1] Wark, D.A. and J.F. Lovering (1977) *PLSC*, 95-112. [2] Simon, J.I. et al. (2005) *EPSL*, 238, 272-283. [3] Young, E.D. et al. (2005) *Science*, 308, 223-227. [4] Yurimoto, H. et al. (1998) *Science*, 282, 1874-1876. [5] Krot, A.N. et al. (2002) *Science*, 295, 1051-1054. [6] Aleon, J. et al. (2007) *EPSL* 263, 114-127. [7] Simon J.I. et al. (2011) *Science*, 2011, 1175-1178. [8] Keller, L.P. and P.R. Buseck (1991) *Science*, 1991, 252, 947-949. [9] Metzler, K., A. et al. (1992) *GCA*, 56, 2873-2897. [10] Jacobsen, B. et al. (2011) *ApJL*, 2011, 731(L28). [11] Fagan, T.J. et al. (2004) *MPS*, 39, 1257-1272. [12] Simon, J.I. and E.D. Young (2011) *EPSL*, 304, 468-482. [13] Clayton, R.N. et al. (1977) *EPSL*, 34, 209-224. [14] Matzel, J.E.P. et al. (2013) *LPSC* Abst. #2632. [15] Bodénan, J.-D. et al. (2013) *Metsoc* Abst. #5187. [16] Simon, S.B. and L. Grossman (2013) *LPSC* Abst. #2793. [17] Simon, J.I. et al. (2012) *LPSC* Abst. #1340. [18] Simon, J.I. et al. (2013) *LPSC* Abst. #1828. [19] McKeegan, K.D. et al. (2011) *Science*, 332, 1528-1532.